

Spin-0 Mott insulator to metal to spin-1 Mott insulator transition in the single-orbital Hubbard model on the decorated honeycomb lattice

H. L. Nourse, Ross H. McKenzie, and B. J. Powell

School of Mathematics and Physics, The University of Queensland, Brisbane, Queensland 4072, Australia

We study the interplay of strong electron correlations and intra-triangle spin exchange at two-thirds filling of the single-orbital Hubbard model on the decorated honeycomb lattice using rotationally invariant slave bosons (RISB). We find that the spin exchange tunes between a spin-1 Mott insulator, a metal, and a spin-0 Mott insulator when the exchange is antiferromagnetic. The Mott insulators occur from effective intra-triangle multi-orbital interactions and are adiabatically connected to the ground state of an isolated triangle. An antiferromagnetic spin exchange, as determined by the Goodenough-Kanamori rules, may occur in coordination polymers from kinetic exchange via the ligands. We characterize the magnetism in the regime where spin-triplets dominate. For small U a spin-1 Slater insulator occurs with antiferromagnetic order between triangles. Magnetism in the spin-1 Mott insulator is described by a spin-1 Heisenberg model on a honeycomb lattice, whose ground state is Néel ordered.

I. INTRODUCTION

The Hubbard model is a paradigm for investigating strongly correlated electron systems [1]. Despite the simplicity of the model - a single-orbital model on a lattice with an on-site Coulomb repulsion - it captures a plethora of correlated properties due to the competition between the kinetic energy and Coulomb repulsion. Of central importance to strongly correlated systems is the Mott metal-insulator transition [2], where at half-filling of the Hubbard model an insulator occurs with an electron localized to a lattice site. The prevailing wisdom is that away from half-filling there is instead a metal.

It has been argued that the single-orbital Hubbard model may hold all of the important ingredients for describing high-temperature superconductivity found in the hole doped cuprates [3, 4] and the organic BEDT-TTF superconductors [5]. However, a single electronic band at the Fermi energy is not typical. Many strongly correlated systems are multi-orbital and originate from d - or f -shell atoms, as is found in most transition metals [6] and the iron-based superconductors [7]. Multi-orbital systems are typically modeled with the Hubbard-Kanamori Hamiltonian [8, 9]. In this model there are many more possibilities because of the increased orbital degrees of freedom. For example, a correlated insulator may be found away from half-filling, with a Hund's interaction that is found to enhance the critical interaction strength of the Mott insulating state [9].

However, increasing the orbital degrees of freedom is not the only way to increase the complexity of strongly correlated systems. For example, the low-energy physics of some coordination polymers have elaborate lattices [10–19]. Many coordination polymers display properties observed in strongly correlated systems, such as bad metals and unconventional superconductivity. Recently, it was shown that decorated lattices support a plethora of strongly correlated phases away from half-filling, despite being described by the single-orbital Hubbard model [20]. One of these surprising states was a Mott insulator on the

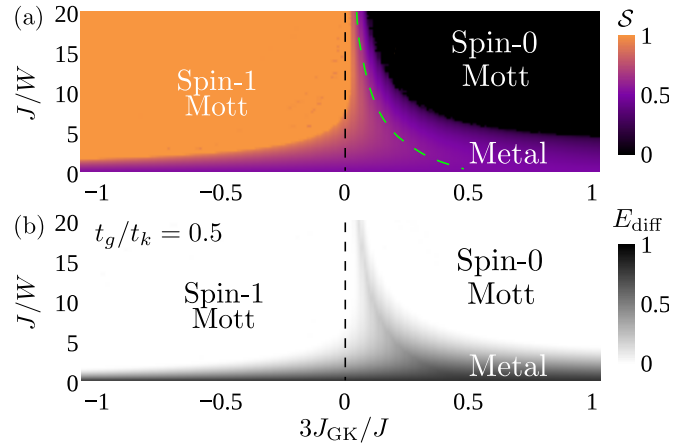


FIG. 1. An intra-triangle spin-exchange J_{GK} tunes between a spin-1 Mott insulator, a metal, and a spin-0 Mott insulator on the decorated honeycomb lattice. The Mott insulators are extended phases from the ground state of an isolated triangle. (a) Effective spin S on a triangle. For $r > 0$ an insulator occurs that forms a total spin-singlet on each triangle, while for $r \leq 0$ there is an effective Hund's interaction that drives spin-triplet formation. The total spin S of a triangle is the solution to $S(S+1) = \sum_i \langle \vec{S}_i \cdot \vec{S}_i \rangle / 2\mathcal{N}$, where the spin operator of triangle i is $\vec{S}_i = \sum_{\alpha=1}^3 \sum_{\sigma\sigma'} \hat{c}_{i\alpha\sigma}^\dagger \vec{\tau}_{\sigma\sigma'} \hat{c}_{i\alpha\sigma'}$, $\vec{\tau}$ is a vector of Pauli matrices, and \mathcal{N} is the number of unit cells on the lattice. (b) Energy per triangle E compared to the ground state energy of an isolated triangle E_0^Δ , $E_{\text{diff}} = E - E_0^\Delta$. The insulators within RISB realize the molecular limit. $J = U + 2J_{\text{GK}}$, the green dashed line marks the boundary between spin-0 and spin-1 ground states of an isolated triangle (cf. Fig. 12), and the dashed black line marks $J_{\text{GK}} = 0$.

decorated honeycomb lattice with spin-triplet formation, denoted as a spin-1 Mott insulator.

Only the screened on-site Coulomb repulsion U is kept in the Hubbard model. However, in many materials, such as coordination polymers, there may be important spin exchange processes that we will show have profound effects. As the spin-1 Mott insulator occurs in the regime

of strong intra-triangle hopping on the decorated honeycomb lattice, we investigate the effect of an intra-triangle spin exchange J_{GK} .

The spin-exchange between sites J_{GK} is determined from kinetic exchange, which in coordinated polymers is mediated by hopping processes between the metal atom or ion and the surrounding ligands. The orientation between the correlated orbitals on the metals and the uncorrelated orbitals on the ligands, combined with the Coulomb exchange on the ligands, dictates whether the overall contribution is antiferromagnetic or ferromagnetic, as may be inferred from the Goodenough-Kanamori rules of superexchange [21–23].

Our central result is summarized in Fig. 1. An antiferromagnetic spin exchange J_{GK} suppresses spin triplet formation on a triangle and there is instead a spin-0 Mott insulator. It is possible to tune between a spin-1 Mott insulator, a metal, and a spin-0 Mott insulator. The sign of J_{GK} may be tuned by uniaxial pressure or chemical substitution. Furthermore, a ferromagnetic J_{GK} highlights that the spin-1 Mott insulator occurs from an effective Hund’s rule coupling and is connected to physics found in the Hubbard-Kanamori model.

The paper is organized as follows: The Hubbard model on the decorated honeycomb lattice is introduced in Section II and presented in the basis of molecular orbitals of a triangle, which we denote the trimer orbitals. We discuss the limit of isolated triangles ($t_g = 0, t_k > 0$) and the limit of infinitely separated in energy trimer orbitals ($t_g/t_k \rightarrow 0, t_g > 0$). Mean-field rotationally invariant slave bosons (RISB) are introduced in Section III, which is the method we use to solve the model. In Section IV we present our results restricted to paramagnetic states and characterize in detail the metal-insulator transition to a Mott insulator with spin-1 formation. In Section V we discuss how an intra-triangle spin exchange can suppress triplet formation on a triangle and instead drive a spin-0 Mott insulator. In Section VI we discuss antiferromagnetic solutions, where a spin-density wave forms between spin-triplet polarized triangles. In Section VII we discuss what the magnetism looks like in the spin-1 Mott insulator. Finally, Section VIII presents our conclusions and the implication of our results for other decorated lattices with triangular structures.

II. THE MODEL

The Hamiltonian for the Hubbard model with an intra-triangle spin-exchange on the decorated honeycomb lat-

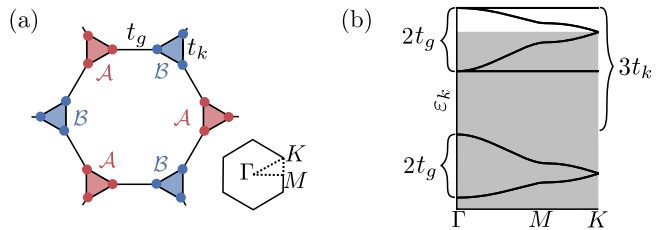


FIG. 2. (a) The decorated honeycomb lattice. The intra-(inter)triangle hopping amplitude is t_g (t_k), and \mathcal{A} and \mathcal{B} label the inequivalent triangles in the unit cell. The inset shows the hexagonal Brillouin zone. Γ , K , and M are the k -points of high symmetry in reciprocal space. (b) Non-interacting band structure of the Dirac metal at two-thirds filling for $t_g/t_k = 0.5$. The dispersion ε_k is shown between the points of high symmetry, and the shaded region indicates electron filling up to the Fermi energy.

tice [24] is

$$\hat{H} \equiv \hat{H}^{\Delta \rightarrow \Delta} + \sum_i \hat{H}_i^{\Delta}, \quad (1)$$

$$\hat{H}^{\Delta \rightarrow \Delta} \equiv -t_g \sum_{\langle i\alpha, j\alpha \rangle, \sigma} \hat{c}_{i\alpha\sigma}^\dagger \hat{c}_{j\alpha\sigma}, \quad (2)$$

$$\hat{H}_i^{\Delta} \equiv \hat{H}_i^0 + \hat{H}_i^U + \hat{H}_i^{\text{GK}}, \quad (3)$$

$$\hat{H}_i^0 \equiv -t_k \sum_{\alpha \neq \beta, \sigma} \hat{c}_{i\alpha\sigma}^\dagger \hat{c}_{i\beta\sigma}, \quad (4)$$

$$\hat{H}_i^U \equiv U \sum_{\alpha} \hat{n}_{i\alpha\uparrow} \hat{n}_{i\alpha\downarrow}, \quad (5)$$

$$\hat{H}_i^{\text{GK}} \equiv J_{\text{GK}} \sum_{\alpha \neq \beta} \left(\vec{S}_{i\alpha} \cdot \vec{S}_{i\beta} - \frac{\hat{n}_{i\alpha} \hat{n}_{i\beta}}{4} \right), \quad (6)$$

where $\hat{c}_{i\alpha\sigma}^\dagger$ ($\hat{c}_{i\alpha\sigma}$) creates (annihilates) an electron with spin $\sigma \in \{\uparrow, \downarrow\}$ on site $\alpha \in \{1, 2, 3\}$ of triangle i , $\hat{n}_{i\alpha\sigma} \equiv \hat{c}_{i\alpha\sigma}^\dagger \hat{c}_{i\alpha\sigma}$, t_g (t_k) is the inter-(intra-)triangle hopping integral (Fig. 2a), $\langle i\alpha, j\alpha \rangle$ signifies nearest-neighbor hopping between sites of adjacent triangles, U is the local Coulomb repulsion, and J_{GK} is the intra-triangle spin exchange.

A. The molecular orbital basis for two-thirds filling

It will be helpful below to consider the molecular orbitals of a triangle, which we denote as the trimer orbitals. To do so we write

$$\hat{c}_{i\alpha\sigma}^\dagger \equiv \frac{1}{\sqrt{3}} \sum_m \hat{b}_{im\sigma}^\dagger e^{-i\phi(\alpha-1)m}, \quad (7)$$

where $\phi = 2\pi/3$, $m \in \{-1, 0, 1\} \equiv \{E_1, A, E_2\}$ labels the trimer orbitals, and $m+m'$ is calculated modulo 3 shifted to the interval $[-1, 1]$. The intra-triangle terms (Eq. (3))

have the representation (Appendices A and B)

$$\hat{H}_i^0 = -2t_k \sum_{m,\sigma} \cos(\phi m) \hat{b}_{im\sigma}^\dagger \hat{b}_{im\sigma}, \quad (8)$$

$$\begin{aligned} \hat{H}_i^U &= -\frac{U}{3} \hat{S}_i^2 + \frac{U}{12} \hat{N}_i^2 + \frac{U}{6} \hat{N}_i - \frac{U}{3} \sum_m \hat{n}_{im\uparrow} \hat{n}_{im\downarrow} \\ &+ \frac{U}{3} \sum_m \sum_{n \neq m} \sum_{p \neq m \neq n} \left(\hat{b}_{im\downarrow}^\dagger \hat{b}_{im\uparrow}^\dagger \hat{b}_{in\uparrow} \hat{b}_{ip\downarrow} + \text{H.c.} \right), \end{aligned} \quad (9)$$

$$\begin{aligned} \hat{H}_i^{\text{GK}} &= \frac{J_{\text{GK}}}{3} \hat{S}_i^2 - \frac{J_{\text{GK}}}{12} \hat{N}_i^2 - \frac{J_{\text{GK}}}{6} \hat{N}_i - \frac{2J_F}{3} \sum_m \hat{n}_{im\uparrow} \hat{n}_{im\downarrow} \\ &+ \frac{2J_{\text{GK}}}{3} \sum_m \sum_{n \neq m} \sum_{p \neq m \neq n} \left(\hat{b}_{im\downarrow}^\dagger \hat{b}_{im\uparrow}^\dagger \hat{b}_{in\uparrow} \hat{b}_{ip\downarrow} + \text{H.c.} \right), \end{aligned} \quad (10)$$

where $\hat{n}_{im\sigma} \equiv \hat{b}_{im\sigma}^\dagger \hat{b}_{im\sigma}$, $\hat{N}_i \equiv \sum_{m,\sigma} \hat{n}_{im\sigma}$, $\vec{S}_i^2 = \vec{S}_i \cdot \vec{S}_i$, $\vec{S}_i = \sum_m \vec{S}_{im}$, and $\vec{S}_{im} = (S_{im}^x, S_{im}^y, S_{im}^z)$ is given by

$$\vec{S}_{im} \equiv \frac{1}{2} \sum_{\sigma\sigma'} \hat{b}_{im\sigma}^\dagger \vec{\tau}_{\sigma\sigma'} \hat{b}_{im\sigma'}, \quad (11)$$

where $\vec{\tau}$ is a vector of Pauli matrices. \hat{H}_i^0 (Eq. (8)) defines the energy of the trimer orbitals, with the degenerate E_1 and E_2 orbitals $3t_k$ higher in energy than the A orbital for $t_k > 0$ (Fig. 3a). One can infer the effect of the interactions by considering the case $J_{\text{GK}} = 0$. The \hat{N}_i^2 term disfavors charge fluctuations on a triangle. The \hat{S}_i^2 term favors maximizing the total spin on a triangle and reflects Hund's first rule. The intra-orbital Coulomb attraction favors low spin configurations and competes with the \hat{S}_i^2 term. The last term in \hat{H}_i^U and \hat{H}_i^{GK} (Eqs. (9) and (10) respectively) describes a three-orbital hopping process that creates (annihilates) double occupancy on an orbital. See Appendices A and B for details.

At two-thirds filling the Hubbard model of an isolated triangle is exactly solvable and is exact within RISB with triangular clusters. For $t_k > 0$, $U > 0$, $J_{\text{GK}} = 0$ the ground state is three-fold degenerate with energy

$$E_0^\Delta(J_{\text{GK}} = 0) = -2t_k + U \quad (12)$$

and the three triplet states are [25]

$$\begin{aligned} |t_i^\uparrow\rangle &\equiv \hat{b}_{iA\uparrow}^\dagger \hat{b}_{iA\downarrow}^\dagger \hat{b}_{iE_1\uparrow}^\dagger \hat{b}_{iE_2\uparrow}^\dagger |0\rangle, \\ |t_i^0\rangle &\equiv \frac{1}{\sqrt{2}} \hat{b}_{iA\uparrow}^\dagger \hat{b}_{iA\downarrow}^\dagger \left(\hat{b}_{iE_1\uparrow}^\dagger \hat{b}_{iE_2\downarrow}^\dagger + \hat{b}_{iE_1\downarrow}^\dagger \hat{b}_{iE_2\uparrow}^\dagger \right) |0\rangle, \\ |t_i^\downarrow\rangle &\equiv \hat{b}_{iA\uparrow}^\dagger \hat{b}_{iA\downarrow}^\dagger \hat{b}_{iE_1\downarrow}^\dagger \hat{b}_{iE_2\downarrow}^\dagger |0\rangle, \end{aligned} \quad (13)$$

where $|0\rangle$ is the vacuum.

The inter-triangle hopping t_g couples the molecular orbitals of adjacent triangles. In the molecular orbital basis Eq. (2) can be written as

$$\hat{H}^{\Delta \rightarrow \Delta} = \sum_m \hat{H}_m^{\text{honeycomb}} + \sum_{m \neq n} \hat{H}_{mn}^{\text{trimer}}, \quad (14)$$

which is a complicated three-orbital tight-binding model on a honeycomb-like lattice (Fig. 3b,c). The first term is the tight-binding model on the honeycomb lattice, given in reciprocal space by

$$\hat{H}_m^{\text{honeycomb}} = \frac{1}{3} \sum_{k\sigma} \vec{\Psi}_{km\sigma}^\dagger \mathcal{H}_k^{\text{honeycomb}} \vec{\Psi}_{km\sigma}, \quad (15)$$

with $\vec{\Psi}_{km\sigma} \equiv (\hat{b}_{1km\sigma}, \hat{b}_{2km\sigma})^T$,

$$\mathcal{H}_k^{\text{honeycomb}} = -t_g \begin{pmatrix} 0 & \Delta_k \\ \Delta_k^* & 0 \end{pmatrix}, \quad (16)$$

where k indexes a vector \vec{k} in reciprocal space, $\ell = \mathcal{A}, \mathcal{B}$ in $\hat{b}_{\ell km\sigma}$ labels the two sites in the unit cell of the honeycomb lattice (Fig. 2a), and $\Delta_k = \sum_{j=1}^3 e^{i\vec{k} \cdot \vec{r}_j}$ with \vec{r}_j denoting the three vectors to the nearest-neighbor sites in real-space (Fig. 3c). The second term between different trimer orbitals takes a similar form but has a direction dependent phase, given by

$$\hat{H}_{mn}^{\text{trimer}} = \frac{1}{3} \sum_{k\sigma} \vec{\Psi}_{km\sigma}^\dagger \mathcal{H}_k^{\text{trimer}} \vec{\Psi}_{kn\sigma}, \quad (17)$$

with

$$\mathcal{H}_k^{\text{trimer}} = -t_g \begin{pmatrix} 0 & \delta_k \\ \delta_k^* & 0 \end{pmatrix}, \quad (18)$$

where $\delta_k = \sum_{j=1}^3 e^{i(\vec{k} \cdot \vec{r}_j + (j-1)\phi)}$.

B. The non-interacting limit

In Fig. 2b we show an example of the non-interacting ($U = 0$, $J_{\text{GK}} = 0$) band structure for $t_g/t_k < 3/2$. At $\vec{k} = \vec{0}$ (the Γ point) the eigenstates of Eq. (1) can be labeled by the trimer orbitals and the (anti-)bonding orbitals of the honeycomb lattice. Hence, at Γ , the (anti-)bonding orbitals cause the two A eigenenergies to be separated in energy by $2t_g$, and the four E eigenenergies that are two-fold degenerate to be separated in energy by $2t_g$. The set of A eigenenergies are lower in energy by $3t_g$ from the the set of E eigenenergies because of the energy difference between the molecular orbitals of an isolated triangle. Away from Γ the labeling is not exact, but the set of lower (upper) bands retain significant A (E) orbital character and are honeycomb-like (Fig. 2b).

In the limit $t_g/t_k \rightarrow 0$ ($t_g \neq 0$) the A and E orbitals are infinitely separated in energy, the upper set of bands decouple from the lower set, and the three-orbital hopping terms in Eqs. (9) and (10) can be neglected. Electrons in the A orbitals are exactly described by the Hubbard model with the intra-triangle spin-exchange on the honeycomb lattice. Electrons in the E orbitals are exactly described by a degenerate two-orbital Hubbard-Kanamori model on a honeycomb-like lattice with phase dependent hopping.

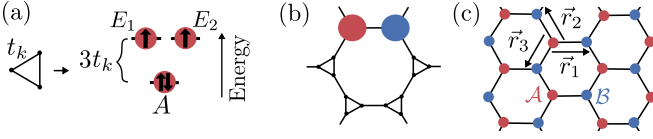


FIG. 3. (a) The trimer orbitals of an equilateral triangle. For $t_k > 0$ the A molecular orbital has lower energy than the two degenerate E molecular orbitals. The ground state of the single-orbital Hubbard model ($J_{\text{GK}} = 0$) of a three-site ring at two-thirds electron filling and $U > 0$ is a spin-triplet. (b) In the basis of the trimer orbitals the decorated honeycomb lattice maps to a three-orbital model on the (c) honeycomb lattice with complicated phase dependent inter- and intra-orbital hopping between trimers. The vectors to nearest neighbor sites is given by $\vec{r}_1 = (\vec{a}_1 + \vec{a}_2)/3$, $\vec{r}_2 = (\vec{a}_1 - 2\vec{a}_2)/3$, and $\vec{r}_3 = (\vec{a}_2 - 2\vec{a}_1)/3$, where the primitive lattice vectors are $\vec{a}_1 = a(3/2, \sqrt{3}/2)$ and $\vec{a}_2 = a(3/2, -\sqrt{3}/2)$, where $a = 1$ is the lattice spacing.

III. METHODS: RISB MEAN-FIELD THEORY

We solve Eq. (1) using mean-field rotationally invariant slave-boson (RISB) theory [26–29] using three-site (triangular) clusters. At the saddle-point level RISB captures the coherent low-energy quasiparticles in metallic states, and captures metal-insulator transitions in the paramagnetic state of multi-orbital systems. Importantly, rotational invariance allows us to work in the molecular orbital basis of a triangle.

In RISB the local physical Hilbert space of a cluster is mapped onto a larger Hilbert space described by auxiliary fermions and bosons. The advantage is that the auxiliary fermions only enter the problem quadratically and can be integrated out, at the expense of an action that depends on the slave bosons and Lagrange multiplier fields, which are evaluated at the saddle-point level.

A new set of auxiliary fermions are introduced for each electronic mode (sites, orbitals, and spin) on a cluster $\{\hat{f}_{ia}|a = 1, \dots, M_i\}$, where $M_i = 6$ is the number of electronic modes on a triangle. There are 2^{M_i} physical states $\{|A_i\rangle\}$ and 2^{M_i} auxiliary fermion states $\{|n_i\rangle\}$ on a cluster. A boson $\hat{\Phi}_{iAn}$ is introduced for each pair of physical and auxiliary fermion state $\{|A_i\rangle, |n_i\rangle\}$, with the restriction that the number of particles in state $|A_i\rangle$, denoted as N_{iA} , is equal to the number of particles in state $|n_i\rangle$, denoted as N_{in} .

In the enlarged Hilbert space, a faithful representation of the physical electron is given by (i indexes a cluster and a a index sites, orbitals, and spin)

$$\hat{c}_{i\alpha}^\dagger \equiv \sum_a \hat{\mathcal{R}}_{ia\alpha} \hat{f}_{ia}^\dagger, \quad (19)$$

with the unitary operator

$$\hat{\mathcal{R}}_{ia\alpha} \equiv \sum_{AB} \sum_{nm} \frac{\langle A|\hat{c}_{i\alpha}^\dagger|B\rangle \langle n|\hat{f}_{ia}^\dagger|m\rangle}{\sqrt{N_{iA}(M_i - N_{iB})}} \hat{\Phi}_{iAn}^\dagger \hat{\Phi}_{iBm}. \quad (20)$$

To restrict the enlarged Hilbert space to only the physical states the following (Gutzwiller) constraints are introduced

$$\hat{K}_i^0 \equiv \sum_{An} \hat{\Phi}_{iAn}^\dagger \hat{\Phi}_{iBn} - \hat{1}, \quad (21)$$

$$\hat{K}_{iab} \equiv \hat{f}_{ia}^\dagger \hat{f}_{ib} - \sum_{Anm} \langle m_i|\hat{f}_{ia}^\dagger \hat{f}_{ib}|n_i\rangle \hat{\Phi}_{iAn}^\dagger \hat{\Phi}_{iAm}, \quad (22)$$

where $\hat{1}$ is the identity. \hat{K}_i^0 enforces that only states with a single boson are retained, while \hat{K}_{iab} enforces that a physical state has the correct bosons attached to their corresponding auxiliary fermion. The constraints are incorporated into the Hamiltonian (Eq. (1)) in the enlarged Hilbert space with Lagrange multipliers E_i^c and λ_{iab} respectively.

With the above restrictions, a physical state in the enlarged Hilbert space is given by

$$|A_i\rangle \equiv \frac{1}{\sqrt{D_{iA}}} \sum_n \hat{\Phi}_{iAn}^\dagger |0\rangle \otimes |n_i\rangle, \quad (23)$$

where $D_{iA} = \binom{M_i}{N_{iA}}$ is the number of auxiliary fermion states with N_{iA} particles. Hence, one can show that any local observable acting on a cluster in the enlarged Hilbert space has a faithful representation given by [27]

$$\hat{X}[\underline{c}_{i\alpha}^\dagger, \underline{c}_{i\alpha}] = \sum_{AB} \langle A|\hat{X}[\hat{c}_{i\alpha}^\dagger, \hat{c}_{i\alpha}]|B\rangle \sum_n \hat{\Phi}_{iAn}^\dagger \hat{\Phi}_{iBn}. \quad (24)$$

At the saddle-point level the bosons condense ($\langle \hat{\Phi}_{iAn} \rangle \rightarrow [\phi_i]_{An}$, $\langle \hat{\mathcal{R}}_{ia\alpha} \rangle \rightarrow [\mathcal{R}_i]_{a\alpha}$), and the constraints are only enforced on average. The local density matrix Δ_i^p of \hat{H}^{qp} (Eq. (28)) and the renormalization matrix \mathcal{R}_i are promoted to free parameters with the Lagrange-Legendre terms

$$\begin{aligned} & [\lambda_i^c]_{ab} \left(\sum_{Anm} \langle n|\hat{f}_{ia}^\dagger \hat{f}_{ib}|m\rangle [\phi_i^\dagger]_{nA} [\phi_i]_{Am} - [\Delta_i^p]_{ab} \right), \quad (25) \\ & [\mathcal{D}_i]_{a\alpha} \left(\sum_{ABnm} \langle A|\hat{c}_{i\alpha}^\dagger|B\rangle \langle m|\hat{f}_{ia}|n\rangle [\phi_i^\dagger]_{nA} [\phi_i]_{Bm} \right. \\ & \quad \left. - \sum_c [\mathcal{R}_i]_{c\alpha} [\Delta_i^p (1 - \Delta_i^p)]_{ca}^{1/2} \right) + \text{H.c.} \quad (26) \end{aligned}$$

where their definitions are enforced with the Lagrange multiplier fields $[\lambda_i^c]_{ab}$ and $[\mathcal{D}_i]_{a\alpha}$ respectively [28, 29]. The resulting mean-field theory is entirely encoded by

the Lagrange functional [30]

$$\begin{aligned}
\mathcal{L}[\mathcal{R}_i, \lambda_i, \Delta_i^p, E_i^c, \mathcal{D}_i, \lambda_i^c, |\Phi_i\rangle] \\
&= \lim_{\beta \rightarrow \infty} \frac{1}{\beta} \sum_{i\omega_n} \text{Tr} \ln \hat{G}^{\text{qp}}(i\omega_n) \\
&+ \sum_i \left[\langle \Phi_i | \hat{H}_i^{\text{emb}} | \Phi_i \rangle + E_i^c (1 - \langle \Phi_i | \Phi_i \rangle) \right] \\
&- \sum_{i, a\alpha c} \left([\mathcal{D}_i]_{a\alpha} [\mathcal{R}_i]_{c\alpha} [\Delta_i^p (1 - \Delta_i^p)]_{ca}^{1/2} + \text{c.c.} \right) \\
&- \sum_{i, ab} \left([\lambda_i]_{ab} + [\lambda_i^c]_{ab} \right) [\Delta_i^p]_{ab}, \quad (27)
\end{aligned}$$

where the auxiliary fermions Green's function is given by $\hat{G}^{\text{qp}}(z) \equiv (z - \hat{H}^{\text{qp}})^{-1}$ with the Hamiltonian

$$\begin{aligned}
\hat{H}^{\text{qp}} \equiv & - \sum_{ij, \alpha\beta, ab} [\mathcal{R}_i]_{a\alpha} [t_{ij}]_{\alpha\beta} [\mathcal{R}_j^\dagger]_{\beta b} \hat{f}_{ia}^\dagger \hat{f}_{jb} \\
& + \sum_{i, ab} [\lambda_i]_{ab} \hat{f}_{ia}^\dagger \hat{f}_{ib}, \quad (28)
\end{aligned}$$

$|\Phi_i\rangle$ is the ground state of the embedding Hamiltonian which is an impurity problem given by the Hamiltonian

$$\begin{aligned}
\hat{H}_i^{\text{emb}} \equiv & \hat{H}_i^\Delta + \sum_{a\alpha} \left([\mathcal{D}_i]_{a\alpha} \hat{c}_{i\alpha}^\dagger \hat{f}_{ia} + \text{H.c.} \right) \\
& + \sum_{ab} [\lambda_i^c]_{ab} \hat{f}_{ib} \hat{f}_{ia}^\dagger, \quad (29)
\end{aligned}$$

where λ_i^c and \mathcal{D}_i are matrices that describe the bath and the hybridization between the bath and the impurity respectively, and E_i^c enforces the normalization of $|\Phi_i\rangle$. The same grand potential can be derived from the Gutzwiller approximation [26, 31–33].

The parameters of the Lagrange functional (Eq. (27)) have to be determined self-consistently. We assume a uniform lattice where each triangle is equivalent and drop the label i . The Lagrange functional is extremized with respect to \mathcal{R} , λ , Δ^p , E^c , \mathcal{D} , λ^c , and $|\Phi\rangle$, leading to the following equations:

$$[\Delta^p]_{ab} = \frac{1}{\mathcal{N}} \left[\sum_k f(\varepsilon_k^{\text{qp}}) \right]_{ba}, \quad (30)$$

$$\begin{aligned}
[\mathcal{D}]_{a\alpha} = & \sum_c [\Delta^p (1 - \Delta^p)]_{ac}^{-1/2} \\
& \times \left[\frac{1}{\mathcal{N}} \sum_k \varepsilon_k \mathcal{R}^\dagger f(\varepsilon_k^{\text{qp}}) \right]_{c\alpha}, \quad (31)
\end{aligned}$$

$$\begin{aligned}
[\lambda^c]_{ab} = & -[\lambda]_{ab} - \frac{1}{2} \left([(\mathcal{R}\mathcal{D})^\text{T}] \right. \\
& \left. \times (\Delta^p (1 - \Delta^p))^{-1/2} (1 - 2\Delta^p) \right]_{ba} + \text{c.c.}, \quad (32)
\end{aligned}$$

$$\hat{H}^{\text{emb}} |\Phi\rangle = E^c |\Phi\rangle, \quad (33)$$

$$\begin{aligned}
[\lambda]_{ab} = & -[\lambda^c]_{ab} - \frac{1}{2} \left([(\mathcal{R}\mathcal{D})^\text{T} \mathbf{N}^f (1 - \mathbf{N}^f)]^{-1/2} \right. \\
& \left. \times (1 - 2\mathbf{N}^f) \right]_{ba} + \text{c.c.}, \quad (34)
\end{aligned}$$

$$[\mathcal{R}]_{a\alpha} = \sum_c [\mathbf{M}^{cf}]_{\alpha c} \left[(\mathbf{N}^f (1 - \mathbf{N}^f))^{-1/2} \right]_{ca}, \quad (35)$$

where ε_k is the dispersion matrix of $\hat{H}^{\Delta \rightarrow \Delta}$ (Eq. (2)), $\varepsilon_k^{\text{qp}}$ is the dispersion matrix of \hat{H}^{qp} (Eq. (28)), $f(\varepsilon)$ is the Fermi function, $[\mathbf{N}^f]_{ab} \equiv \langle \Phi | \hat{f}_b \hat{f}_a^\dagger | \Phi \rangle$, and $[\mathbf{M}^{cf}]_{\alpha a} \equiv \langle \Phi | \hat{c}_\alpha^\dagger \hat{f}_a | \Phi \rangle$. The RISB saddle-point equations are solved by the following procedure: (i) guess λ , \mathcal{R} and construct \hat{H}^{qp} (Eq. (28)); (ii) solve Eqs. (30)–(32) for Δ^p , \mathcal{D} , and λ^c ; (iii) construct \hat{H}^{emb} (Eq. (29)) and solve the resulting Hamiltonian (Eq. (33)) for the ground state $|\Phi\rangle$; (iv) evaluate \mathbf{N}^f , \mathbf{M}^{cf} and solve Eqs. (34) and (35) for a new guess for λ and \mathcal{R} ; (v) repeat until λ and \mathcal{R} converge.

At the saddle-point level the physical electrons Green's function is a matrix given by

$$\begin{aligned}
\mathbf{G}(k, \omega) \equiv & \mathcal{R}^\dagger \mathbf{G}^{\text{qp}}(k, \omega) \mathcal{R} \\
& = \left[\omega (\mathcal{R}^\dagger \mathcal{R})^{-1} - \mathcal{R}^{-1} \lambda \mathcal{R}^{\dagger -1} - \varepsilon_k \right]^{-1} \\
& = [\omega \mathbf{1} - \varepsilon_k - \varepsilon^0 - \Sigma(\omega)]^{-1}, \quad (36)
\end{aligned}$$

where the self-energy is

$$\Sigma(\omega) = \omega (\mathbf{1} - (\mathcal{R}^\dagger \mathcal{R})^{-1}) + \mathcal{R}^{-1} \lambda \mathcal{R}^{\dagger -1} - \varepsilon^0, \quad (37)$$

and ε^0 are the one-body terms in \hat{H}^Δ , Eq. (3). The spectral function matrix $\mathbf{A}(k, \omega) \equiv -\pi^{-1} \text{Im} \mathbf{G}(k, \omega)$ is given by

$$\mathbf{A}(k, \omega) = \mathcal{R}^\dagger \delta(\omega \mathbf{1} - \varepsilon_k^{\text{qp}}) \mathcal{R}, \quad (38)$$

so that the spectral weight in the orbitals is obtained as

$$\int_{-\infty}^{\infty} d\omega [\mathbf{A}]_{\alpha\beta}(k, \omega) = [\mathbf{R}^\dagger \mathbf{R}]_{\alpha\beta} = [\mathbf{Z}]_{\alpha\beta}, \quad (39)$$

where the quasiparticle weight matrix is given by

$$\mathbf{Z} \equiv \left(\mathbf{1} - \frac{\partial \text{Re} \Sigma(\omega)}{\partial \omega} \Big|_{\omega=0} \right)^{-1} = \mathcal{R}^\dagger \mathcal{R}. \quad (40)$$

It is easily checked that the quantities of the physical electron $\mathbf{G}(k, \omega)$, $\Sigma(\omega)$, $\mathbf{A}(k, \omega)$, and \mathbf{Z} are gauge invariant [27]. We present the results below in the trimer basis of a triangle (Fig. 3a), which elucidates the connection to the ground state of an isolated triangle and the physical mechanism of the spin-1 Mott insulator.

We implemented RISB within the TRIQS library [34, 35]. The k -integrals were evaluated using the linear tetrahedron method [36], and the impurity was solved using exact diagonalization using the Arnoldi method in

ARPACK-NG [37, 38]. On the embedding state $|\Phi\rangle$ and mean-field matrices λ , \mathcal{R} , λ^c , and Δ^p , we imposed the symmetry of \hat{H}_i^Δ including the \mathcal{C}_3 rotational symmetry of a triangle, but not the full $SU(2)$ symmetry when investigating antiferromagnetic solutions. The matrices are block diagonal in spin, and in the trimer basis are block diagonal in the trimer orbitals A , E_1 , and E_2 , where the matrix elements for E_1 and E_2 are equivalent because of the \mathcal{C}_3 symmetry (and we denote either by E).

IV. SPIN-1 MOTT METAL-INSULATOR TRANSITION: PARAMAGNETIC SOLUTIONS

We first investigate paramagnetic solutions obtained within RISB. We will show that there is a Mott metal-insulator transition to a spin-1 state with a vanishing quasiparticle weight on the decorated honeycomb lattice. In the spin-1 Mott insulator electrons become localized to a triangle and within RISB charge fluctuations between triangles are frozen. The spin-1 Mott insulator is adiabatically connected to the limit of isolated triangles.

This is the usual description of a Mott insulator captured in slave boson theories [26], and originally described by Brinkman and Rice for the half-filled Hubbard model [39]. We highlight that our results will show that the spin-1 Mott metal-insulator transition is first order (Fig. 4), which differs from the Brinkman-Rice mechanism which is continuous. Furthermore, the description within RISB is richer than a simpler single-site theory because correlations renormalize the quasiparticle bands by different amounts, which is essential to capture the spin-1 Mott insulator.

The spin-1 Mott insulator occurs for a wide range of J_{GK} (Fig. 1). We provide detailed results for $J_{\text{GK}} = 0$, but qualitatively similar results are found for $J_{\text{GK}} \leq 0$. This corresponds to the single-orbital Hubbard model on the decorated honeycomb lattice.

A. Renormalized hopping amplitudes

A useful way to interpret results within RISB is with the auxiliary fermions of the theory, which are described by the Hamiltonian \hat{H}^{qp} (Eq. (28)). Within this picture RISB maps the interacting system to a non-interacting Hamiltonian with parameters renormalized due to the weights of local electronic configurations on a triangle.

At $U = 0$ \hat{H}^{qp} coincides with the physical Hamiltonian (Eq. (1)) because $\mathcal{R} = \mathbf{1}$ and $\lambda = \epsilon^0$, where ϵ^0 are the one-body terms in \hat{H}^Δ . When interactions are turned on the parameters are renormalized. The renormalized inter-trimer hopping terms are given by the matrix $\mathbf{t}_{ij}^* \equiv \mathcal{R} \mathbf{t}_{ij} \mathcal{R}^\dagger$, and the renormalized intra-trimer terms are captured in the matrix λ .

The matrices \mathcal{R} and λ are block diagonal in the A and E orbital representation of a trimer for states that do not

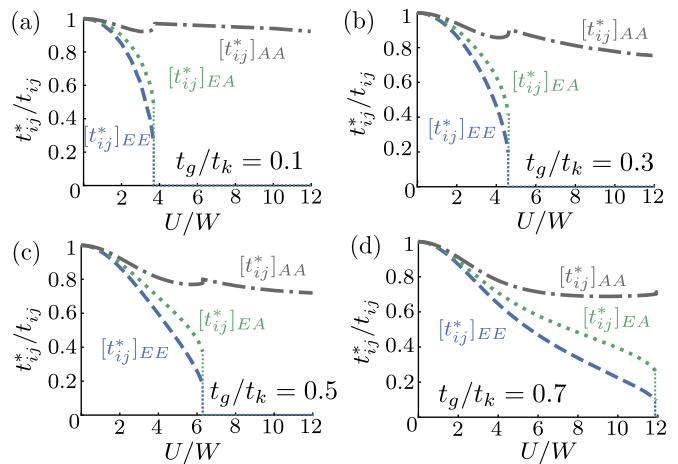


FIG. 4. Metal-insulator transition. Renormalized inter-triangle hopping amplitudes in the trimer basis in the paramagnetic state, given by $[\mathbf{t}_{ij}^*]_{mn} = [\mathcal{R}_i \mathbf{t}_{ij} \mathcal{R}_j^\dagger]_{mn}$, where $m, n = A, E$. In the insulator hopping between the E trimer orbitals of adjacent triangles vanishes while hopping between the A orbitals remains finite. The non-interacting bandwidth is $W = 2t_g$.

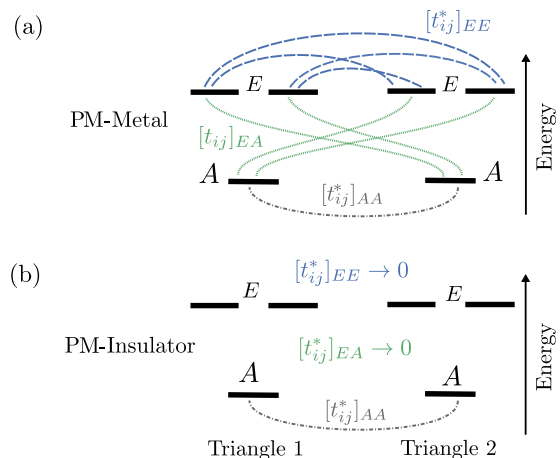


FIG. 5. Schematic of the renormalized inter-triangle hopping parameters in the trimer basis in the paramagnetic (PM) state. (a) The hopping parameters remain finite between all trimer orbitals of adjacent triangles in the metal. (b) Inter-triangle hopping involving the E orbitals of a trimer vanishes in the insulating phase.

break the \mathcal{C}_3 rotational symmetry of a triangle. The correlation potential matrix λ captures the energy difference between the A and degenerate E trimer orbitals, given by $[\lambda]_E - [\lambda]_A$. Hence, an auxiliary fermion can only hop between the A and E orbitals by hopping to an adjacent triangle with amplitude $[\mathbf{t}_{ij}^*]_{AE} = [\mathbf{t}_{ij}^*]_{EA}$.

There is a metal-insulator transition signaled by vanishing hopping between triangles. At the transition $[\mathcal{R}]_{EE} \rightarrow 0$, resulting in $[\mathbf{t}_{ij}^*]_{EE} = [\mathbf{t}_{ij}^*]_{AE} = [\mathbf{t}_{ij}^*]_{EA} = 0$, while $[\mathbf{t}_{ij}^*]_{AA} \neq 0$ (Fig. 4). The A and E orbitals decouple (Fig. 5). Even though $[\mathbf{t}_{ij}^*]_{AA} \neq 0$, the lower set of bands

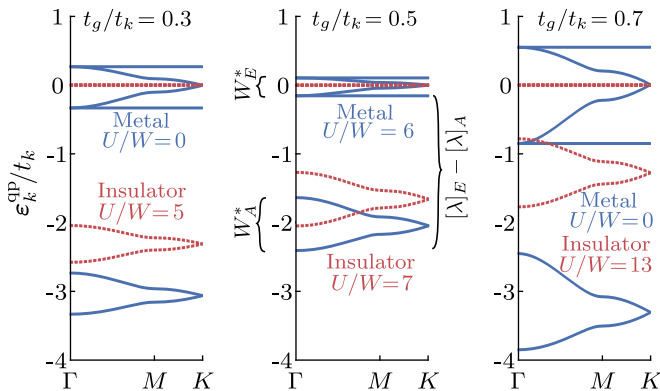


FIG. 6. The renormalized bandwidth $W_E^* \equiv 2[t_{ij}^*]_{EE}$ associated with the set of E bands narrows as correlations increase and are flat in the insulator, while the renormalized bandwidth $W_A^* \equiv 2[t_{ij}^*]_{AA}$ associated with the A bands remains finite and fully occupied. The dispersion $\varepsilon_k^{\text{qp}}$ are the eigenenergies of the auxiliary fermion Hamiltonian Eq. (28).

in the insulator have only A orbital character and are fully occupied at two-thirds filling. Hence, in the auxiliary fermion system there is no hopping between clusters and there are four auxiliary fermions localized to each triangle.

The vanishing hopping between triangles results in flat bands at the Fermi energy in the spectrum of the auxiliary fermions. The E and A bands (Section II) have bandwidths $W_E^* \equiv 2[t_{ij}^*]_{EE}$ and $W_A^* \equiv 2[t_{ij}^*]_{AA}$ respectively, and are separated in energy by $|\lambda|_E - |\lambda|_A$. As the insulator is approached from the metallic side the bands narrow until $W_E^* \rightarrow 0$ at the transition, while W_A^* has finite bandwidth but is fully occupied (Fig. 6). Hence, the spectrum of the auxiliary fermions has flat bands at the Fermi energy, signifying that the state is insulating.

B. Quasiparticle weight and quasiparticle bands

While the auxiliary fermions provide insight into the metal-insulator transition, the spectrum of \hat{H}^{qp} is not equivalent to the spectrum of the physical electron. Instead, the real spectrum is made up of many-body excitations given by the unitary transformation Eq. (19) and captured by the renormalization matrix \mathcal{R} . Within RISB the result is a quasiparticle description, whose propagator is given by the physical electron Green's function (Eq. (36)) and is entirely coherent.

One can understand the effect of correlations on electrons by considering the spectral function (Eq. (38)). Within RISB the coherent part of the single-particle spectral function, as measured in angle-resolved photoe-

mission spectroscopy (ARPES), is given by

$$\begin{aligned} A(k, \omega) &\equiv -\pi^{-1} \text{ImTr} \mathbf{G}(k, \omega) \\ &= \text{Tr}(\mathcal{R}^\dagger \delta(\omega \mathbf{1} - \varepsilon_k^{\text{qp}}) \mathcal{R}) \\ &= \sum_p Z_p^{\text{qp}} \delta(\omega - \varepsilon_{kp}^{\text{qp}}), \end{aligned} \quad (41)$$

where the quasiparticle weight in band p is

$$Z_p^{\text{qp}} \equiv [\mathbf{U}^\dagger(k) \mathbf{Z} \mathbf{U}(k)]_{pp}, \quad (42)$$

with the spectral weight in the orbitals (Eq. (39)) given by $\mathbf{Z} = \mathcal{R} \mathcal{R}^\dagger = \mathcal{R}^\dagger \mathcal{R}$ because \mathcal{R} is unitary, and $\mathbf{U}(k)$ is the single-particle unitary transformation that diagonalizes \hat{H}^{qp} (Eq. (28)) with eigenenergies $\varepsilon_{kp}^{\text{qp}}$, $Z_p^{\text{qp}} \in [0, 1]$, with $Z_p^{\text{qp}} = 1$ corresponding to the non-interacting problem ($U = 0$), and increasing correlations generically decreases Z_p .

At two-thirds filling the quasiparticle weight $[\mathbf{Z}]_E$ in the E orbitals of a trimer approximates the quasiparticle weight of the bands near the Fermi energy [20]. Hence, $[\mathbf{Z}]_E$ is a measure of the metallicity of the system, with $[\mathbf{Z}]_E > 0$ corresponding to a metal and $[\mathbf{Z}]_E = 0$ to a correlated insulator. A vanishing quasiparticle weight signifies a breakdown of the Fermi liquid with a vanishing quasiparticle peak at the Fermi energy in the single-particle spectral function $A(\omega)$ of the electrons (Eq. (41)).

In Fig. 7 we show the quasiparticle weight in the trimer orbitals for different hopping ratios t_g/t_k . The transition from a Dirac metal to a Mott insulator is indicated by a vanishing $[\mathbf{Z}]_E$ (Fig. 7a)]. Even though $[\mathbf{Z}]_A$ remains finite in the insulator (Fig. 7b) it characterizes the spectral weight in quasiparticle bands away from the Fermi energy that are fully occupied. For $t_g/t_k \gtrsim 0.86$ there is no insulator for finite U and there instead is a correlated metal. The insulator is driven either by electronic correlations, or moving towards the molecular limit by lowering t_g/t_k .

In Fig. 8 we show the corresponding spectral function $A(k, \omega)$ as the metal-insulator transition is approached. The quasiparticle bands are given by the spectrum of \hat{H}^{qp} (cf. Section IV A): \mathbf{Z} narrows the bandwidth by renormalizing the inter-cluster hopping and λ shifts the position of the bands. The spectral weight in each band is reduced because of the renormalization by \mathbf{Z} and in the insulator vanishes for the bands at the Fermi energy.

C. Spin-1 formation on a triangle

We now wish to characterize the Mott insulating phase by looking at the local properties on a triangle. As U increases the charge and spin fluctuations on a triangle are suppressed, vanishing at the metal-insulator transition (Fig. 9). In the Mott insulator, electrons become localized to a triangle with four electrons per triangle.

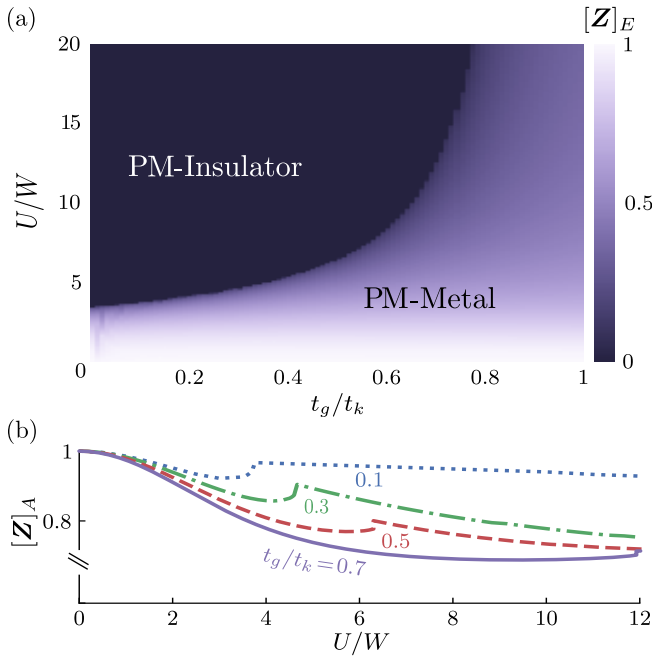


FIG. 7. The metal-insulator transition can be driven by correlations (U) or moving towards the molecular limit ($t_g/t_k \rightarrow 0$), as signified by vanishing elements of the quasiparticle weight matrix \mathbf{Z} in the trimer basis. (a) In the paramagnetic (PM) insulator the quasiparticle weight associated with the E molecular orbitals $[\mathbf{Z}]_E$ discontinuously vanishes. (b) $[\mathbf{Z}]_A$ does not vanish. However, the A molecular orbitals are fully occupied in the insulator (cf. Fig. 10a). There is no Mott insulator for $t_g/t_k \gtrsim 0.86$.

Charge and spin fluctuations between triangles are completely frozen out in the RISB approximation.

In the trimer basis, the effective Coulomb repulsion $U/3$ suppresses intra-orbital charge and spin fluctuations (Fig. 10b,d). Electrons become localized to the A and E orbitals in the insulator, with the A orbitals fully occupied and two electrons shared by the degenerate E orbitals (Fig. 10a).

The electrons localized to the E orbitals act as effective spin-1/2 degrees of freedom (Fig. 10c), and combine to form a total spin-triplet on each triangle (Fig. 11). When there are four electrons per triangle $\mathcal{S} = 0$ indicates only spin-singlets while $\mathcal{S} = 1$ indicates spin-triplet electronic configurations. Hence, we denote the insulator as a spin-1 Mott insulator.

RISB captures the insulator as the molecular limit ($t_g/t_k \rightarrow 0$) of Eq. (1), similarly to how Kotliar-Ruckenstein captures a Mott insulator at half-filling as the atomic limit with no spin fluctuations. One can see this by looking at the parameters of the embedding Hamiltonian (Eq. (29)) in the insulator. Within RISB the energy per triangle is given by

$$E \equiv \sum_{\alpha\alpha'} [\mathcal{D}]_{\alpha\alpha'} \langle \Phi | \hat{c}_{\alpha'}^\dagger \hat{f}_\alpha | \Phi \rangle + \langle \Phi | \hat{H}^\Delta | \Phi \rangle. \quad (43)$$

In the insulator all elements of \mathcal{D} are numerically zero so

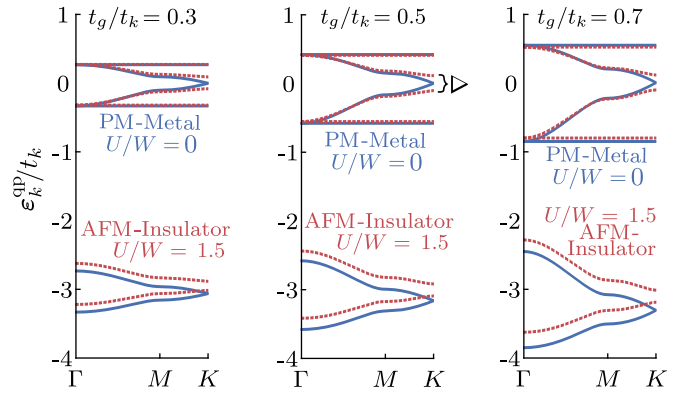


FIG. 8. Spectral weight vanishes in the quasiparticle bands near the Fermi energy ($\omega = 0$) at the metal-insulator transition. The bands are given by the spectrum of the auxiliary fermions (cf. Fig. 6) with spectral weight $A(k, \omega)$ renormalized by the quasiparticle weight. A broadening factor of $+i\eta = i0.025t_k$ was used because the self-energy $\Sigma(\omega)$ is real in the mean-field RISB approximation.

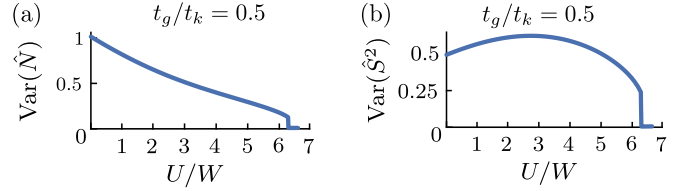


FIG. 9. (a) Charge and (b) spin fluctuations on a triangle vanish in the paramagnetic insulator because electrons become localized within a triangle. The variance of a generic local operator \hat{X} is $\text{Var}(\hat{X}) = \sum_i (\hat{X}_i - \langle \hat{X}_i \rangle)^2 / 2\mathcal{N}$, where $\hat{X}_i = \sum_{\alpha=1}^3 \hat{X}_{i\alpha}$, and \mathcal{N} is the number of unit cells on the lattice. The total particle number operator of triangle i is $\hat{N}_i = \sum_{\alpha=1}^3 \sum_{\sigma} \hat{n}_{i\alpha\sigma}$.

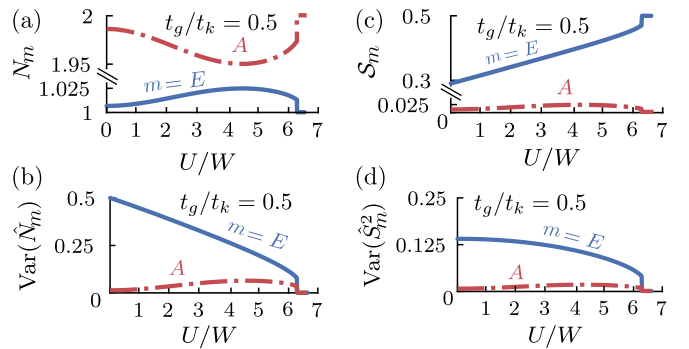


FIG. 10. (a) Number of particles in orbital m of a trimer. In the insulator the A orbital is fully occupied and there are two electrons shared between the E orbitals. (b) Charge fluctuations of a trimer orbital vanish in the insulator in the RISB approximation. (c) Total spin in the trimer orbitals. In the insulator the electrons localized to the E orbitals are pseudo-spin-1/2 moments, and combine to form spin-triplets (cf. Fig. 11). (d) Spin fluctuations of a trimer orbital vanish in the insulator in the RISB approximation.

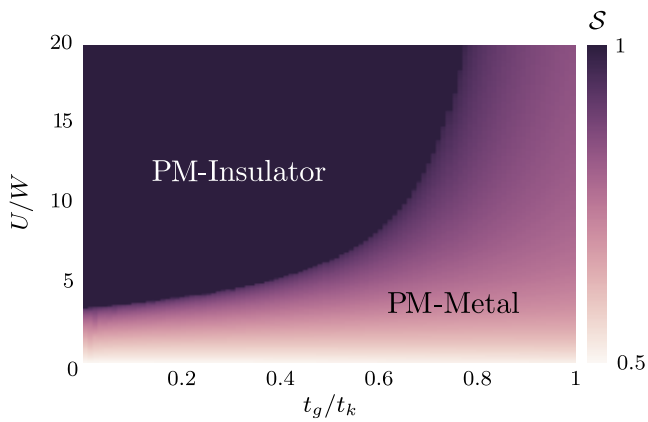


FIG. 11. Increasing interactions favors spin-triplet electronic configurations on a triangle. Spin-1 moments form in the Mott insulator.

that the impurity decouples from the bath. The impurity state $|\Phi\rangle$ of the insulator is a spin-triplet on each triangle with four electrons and is an eigenstate of \hat{H}^Δ . Hence, the ground state energy per triangle in the paramagnetic insulator is equivalent to the ground state energy of an isolated triangle, given by Eq. (12).

Therefore, the spin-1 Mott insulator is an extended phase from the ground state of an isolated triangle where inter-triangle coupling is not sufficient to destroy spin-triplet formation arising from strong correlations. Because the spin-1 Mott insulator realizes the molecular limit, a minimal model of the metal-insulator transition may be captured by a degenerate two-orbital Hubbard-Kanamori model (Section IIB).

V. SPIN-STATE TRANSITIONS FROM INTRA-TRIANGLE SPIN EXCHANGE

In this section we investigate the effect of intra-triangle spin exchange J_{GK} (Eq. (6)). We will show that J_{GK} can drive a spin-state transition from a spin-1 Mott insulator via a metallic phase to a spin-0 Mott insulator for an antiferromagnetic coupling ($J_{\text{GK}} > 0$). This highlights that the spin-1 Mott insulator is driven by an effective Hund's rule coupling that favors spin-triplet formation on a triangle. The spin-state transition can be simply understood from the energetics in the limit of isolated triangles.

To elucidate the effect of J_{GK} it is useful to introduce $J \equiv U + 2J_{\text{GK}}$ and $r \equiv 3J_{\text{GK}}/J$, so that r controls the relative strength of the total spin \hat{S}_i^2 term. The local interactions on a triangle (Eqs. (9) and (10)) can be written

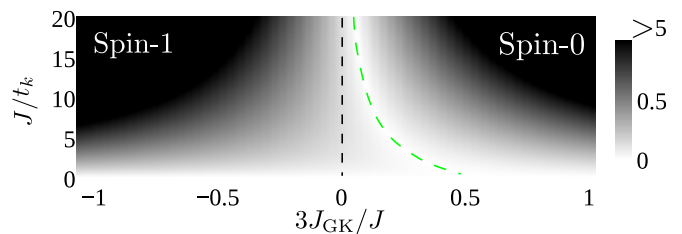


FIG. 12. Spin-state transitions induced by intra-triangle spin exchange J_{GK} on an isolated triangle at two-thirds filling. The green dashed line denotes the boundary between the spin-0 and spin-1 ground states, the colormap is the absolute energy difference between the lowest energy spin-0 and lowest energy spin-1 states, and the black dashed line is the Hubbard model where $J_{\text{GK}} = 0$.

as

$$\begin{aligned} \hat{H}_i^U + \hat{H}_i^J = & -\frac{J}{3}\hat{S}_i^2(1-r) + \frac{J}{12}(1-r)\hat{N}_i^2 \\ & + \frac{J}{6}(1-r)\hat{N}_i - \frac{J}{3}\sum_m \hat{n}_{im\uparrow}\hat{n}_{im\downarrow} \\ & + \frac{J}{3}\sum_m \sum_{n \neq m} \sum_{p \neq m \neq n} \left(\hat{b}_{im\downarrow}^\dagger \hat{b}_{im\uparrow}^\dagger \hat{b}_{in\uparrow} \hat{b}_{ip\downarrow} + \text{H.c.} \right). \end{aligned} \quad (44)$$

When there are four electrons on a triangle, r controls the relative strength of the S_i^2 term, which favors spin-singlets over spin-triplets when it is positive. We also highlight that at $U = -2J_{\text{GK}}$ Eq. (44) is equivalent to the Hubbard-Kanamori Hamiltonian, up to a constant, for the parameters $U' = U - J$, $U = 19J/2$, $J_P = 0$, and $J_X = J$ (see Eq. 5 in [9]).

One can gain insight into the overall effect of J_{GK} by considering an isolated triangle. In Fig. 12 we show the energy difference between the spin-singlet and spin-triplet states, which identifies the ground state. Roughly, for large J a spin-triplet (spin-singlet) ground state is favored for $r \leq 0$ ($r > 0$). For J small enough a spin-triplet is favored even for $r < 1/2$, but one can check numerically that the boundary between the spin-singlet and spin-triplet approaches $r = 0$ as $J \rightarrow \infty$.

In Fig. 1a we show the effect of varying r on the decorated honeycomb lattice for $t_g/t_k = 0.5$. For $r < 0$ the \hat{S}_i^2 term in Eq. (44) reflects Hund's first rule which drives spin-triplet formation on a triangle and lowers the critical interaction strength of the metal-insulator transition. This effect is similarly observed in Hund's metals at half-filling [9, 27]. The insulator at $r < 0$ is in the same phase as the spin-1 Mott insulator at $r = 0$. For $r > 0$ an insulator still occurs for sufficiently large J , but each triangle forms a total spin-0 configuration. Both insulators are extended phases from the ground state of an isolated triangle (Fig. 1b).

Hence, it is possible to tune the system between a spin-1 Mott insulator, a metal, and a spin-0 Mott insulator. As the sign of J_{GK} is determined from the orientation of the ligands, such a tuning may be achieved by uniaxial

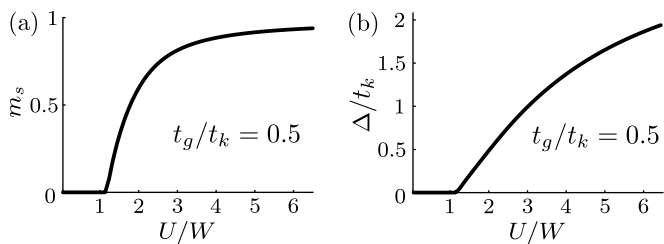


FIG. 13. There is an instability towards antiferromagnetism, signified by the (a) staggered order parameter m_s between adjacent triangles and a (b) gap Δ opening in the quasiparticle bands (cf. Fig. 15).

pressure or chemical substitution.

VI. SPIN-1 SLATER METAL-INSULATOR TRANSITION: ANTIFERROMAGNETIC SOLUTIONS

We now describe the magnetically ordered states captured within RISB. We will show that there is a Slater insulator [40] caused by a spin-density wave (SDW) between adjacent spin-1 polarized triangles which opens a gap in the quasiparticle spectrum. The Slater insulator occurs at a smaller critical interaction strength than the Mott insulator presented in Section IV. The ordered state occurs because of an energy cost for double occupancy so that it becomes energetically favorable to arrange each spin on separate sublattices \mathcal{A} and \mathcal{B} . A SDW lowers the overall energy compared to a paramagnetic metal by lowering the energy of the highest occupied quasiparticle band.

To capture the antiferromagnetic order we allow the set of inequivalent triangles \mathcal{A} and \mathcal{B} (see Fig. 2a) to be described by a different embedding state $|\Phi_\ell\rangle$ (see Eq. (33)) where $\ell = \mathcal{A}, \mathcal{B}$. However, only a single embedding state has to be solved because the magnetic order between triangles at the mean-field level can be accounted for by using the unitary transformation

$$U_\ell = e^{i\phi_\ell \tau^y / 2}, \quad (45)$$

where $\phi_\ell = 0$ (π) for $\ell = \mathcal{A}$ (\mathcal{B}), and τ^y is the Pauli matrix. The transformation can be described by a 2×2 matrix which acts on the spin degrees of freedom and transforms the mean-field matrices as

$$\begin{aligned} [\lambda_{\mathcal{B}}]_m &= U_{\mathcal{B}}^\dagger [\lambda_{\mathcal{A}}]_m U_{\mathcal{B}}, \\ [\mathcal{R}_{\mathcal{B}}]_m &= U_{\mathcal{B}}^\dagger [\mathcal{R}_{\mathcal{A}}]_m U_{\mathcal{B}}. \end{aligned} \quad (46)$$

In Fig. 13a we show the staggered order parameter, given by

$$m_s \equiv \frac{1}{2\mathcal{N}} \left| \sum_i (-1)^{\eta(i)} \langle \hat{S}_i^z \rangle \right|, \quad (47)$$

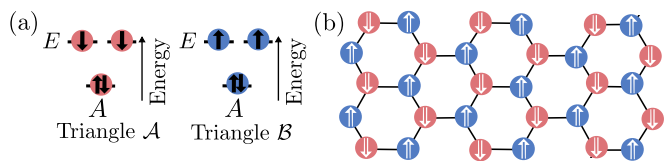


FIG. 14. Schematic of the spin-1 antiferromagnetic ground state. (a) Spin polarized spin-triplet configurations form in the antiferromagnetic insulator and (b) alternate on each triangle.

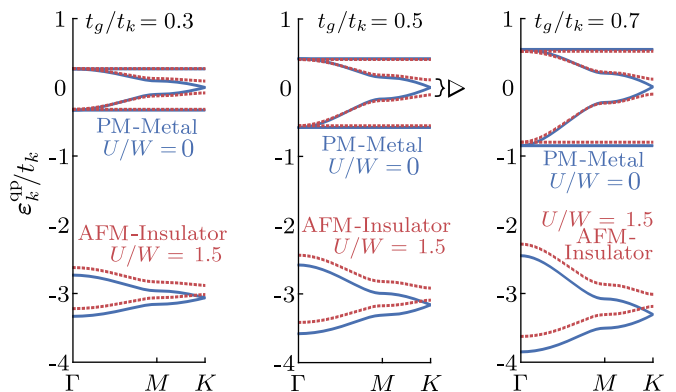


FIG. 15. (a) Band structure of the auxiliary fermions in the antiferromagnetic (AFM) state. In the paramagnetic (PM) Dirac metal the Fermi energy is at the high symmetry point K . In the insulator the inversion symmetry about the center of the bond between adjacent triangles is broken and a gap Δ opens (cf. Fig. 13b). The gap Δ is given by the energy difference between the highest occupied band and the lowest unoccupied band.

where \mathcal{N} is the number of unit-cells, and $\eta(i) = 0$ (1) if the triangle is on sublattice \mathcal{A} (\mathcal{B}). A finite m_s signifies the formation of a SDW on the decorated honeycomb lattice (Fig. 14) due to spin polarization on a triangle. When $m_s \rightarrow 1$ the triangles are fully polarized and there are only $S_z = \pm 1$ spin-triplet electronic configurations. At the onset of antiferromagnetism a gap Δ opens continuously at the Fermi energy (Fig. 13(b)), where Δ is the energy difference between the lowest unoccupied and highest occupied quasiparticle band.

In Fig. 15 we show the spectrum of auxiliary fermions (Eq. (28)) for the antiferromagnetic insulator. The energy is lowered by opening a gap Δ at the high symmetry point K , which occurs because antiferromagnetic order breaks the inversion symmetry about the t_g bond between triangles. In the paramagnetic solutions the Mott insulator occurred from a vanishing quasiparticle weight for the bands near the Fermi energy (Section IV B). In contrast, the quasiparticle weight in the antiferromagnetic insulator remains finite (Fig. 16). Instead, the broken symmetry opens a gap and there is a magnetic band insulator.

The antiferromagnetic insulator which occurs in the RISB theory of the decorated honeycomb lattice is crucially different to the description first proposed by Slater

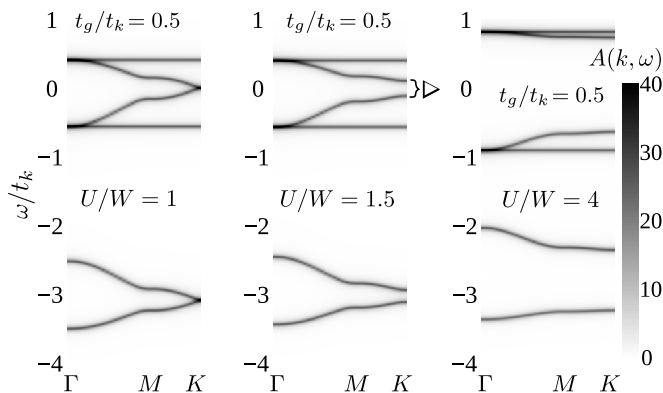


FIG. 16. Quasiparticle bands in the antiferromagnetic state. The bands occur at the spectrum of the auxiliary fermions (cf. Fig. 15) with spectral weight $A(k, \omega)$ renormalized by the quasiparticle weight. In the antiferromagnetic insulator a gap Δ opens at the high symmetry point K (cf. Fig. 13b). Unlike the paramagnetic insulator the spectral weight near the Fermi energy does not vanish (cf. Fig. 8). A broadening factor of $+i\eta = i0.025t_k$ was used because the self-energy $\Sigma(\omega)$ is real in the mean-field RISB approximation.

using Hartree-Fock theory. First, the SDW forms even though the lattice is not at half-filling. Second, the decorated honeycomb lattice is not bipartite and does not have perfect nesting. Hence, the insulator occurs at finite U rather than for any $U > 0$. Third, the spin-1 antiferromagnetic state is beyond a single-site Hartree-Fock description with ordering between sites. Instead, on the decorated honeycomb lattice spin-triplets form because of the effective Hund's interaction, with antiferromagnetic order between triangles. Fourth, usually a Slater insulator has a doubling of the unit-cell associated with the magnetic sublattice. However, because the SDW forms between triangles the magnetic sublattice has the same periodicity as the decorated honeycomb lattice.

In Fig. 17 we compare the energy of the antiferromagnetic insulator with the paramagnetic metal and the paramagnetic insulator. For $U/W \gtrsim 1$ the antiferromagnetic insulator has the lowest energy and is the ground state. The Slater insulator occurs at a lower critical interaction strength than the paramagnetic spin-1 Mott insulator. However, we have only incorporated the antiferromagnetic order at the mean-field level, which ignores important quantum fluctuations that may suppress the formation of a SDW. It is also possible that there is a transition from the SDW to a Néel ordered state arising from the Mott insulator. Larger clusters of the lattice or incorporating fluctuations about the saddle-point [30, 41, 42] may elucidate this issue.

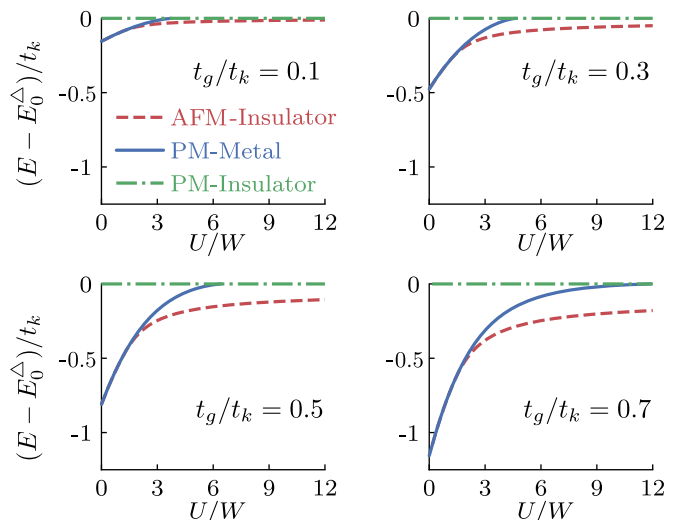


FIG. 17. Energy per triangle comparisons of the different solutions within RISB. The antiferromagnetic (AFM) insulator is the ground state for $U/W \gtrsim 1$ and occurs before the paramagnetic (PM) insulator. The energy of the PM insulator is equivalent to the ground state of an isolated triangle at two-thirds filling, given by $E_0^\Delta(J_{\text{GK}} = 0) = -2t_k + U$.

VII. LOW-ENERGY EFFECTIVE THEORY FOR MAGNETISM IN THE SPIN-1 MOTT INSULATOR

The spin-1 Mott insulator on the decorated honeycomb lattice is adiabatically connected to the ground state of an isolated triangle: there are four electrons on each triangle that form a spin-triplet and inter-triangle charge and spin fluctuations vanish. However, the insulator described by RISB is an incomplete description of the true ground state of the spin-1 Mott state. Within the small cluster choice of our work, slave bosons ignore important higher order energy processes. Going beyond the slave boson approximation would include quantum fluctuations necessary to, e.g., capture the superexchange between triangles.

Hence, we propose that the low-energy effective theory of the insulator is described by the antiferromagnetic spin-1 Heisenberg model on the honeycomb lattice [43–45], given by

$$\hat{H}^{\text{eff}} = J_1 \sum_{\langle ij \rangle} \vec{S}_i \cdot \vec{S}_j + J_2 \sum_{\langle\langle ij \rangle\rangle} \vec{S}_i \cdot \vec{S}_j, \quad (48)$$

where we include a nearest-neighbor J_1 and next-nearest-neighbor J_2 coupling. From perturbation theory to first order in $1/U$ and second order in \hat{H}^{kin} [43] J_1 is given by

$$J_1 = \frac{44t_g^2}{81U} + \frac{2t_g^2 J_{\text{GK}}}{81t_k^2}, \quad (49)$$

and $J_2/J_1 \approx 0.37(t_g/U)^2$. For $J_1 > 0$, $J_2 = 0$ the ground state of the spin-1 Heisenberg model on the honeycomb lattice is Néel ordered [46–49].

On a frustrated honeycomb lattice where $J_2/J_1 > 0$ the picture is less clear. A density matrix renormalization group (DMRG) study [46] suggests a possible plaquette valence-bond crystal for $0.27 < J_2/J_1 < 0.32$ between the Néel ordered state and a spiral AFM, which is supported by a coupled cluster study [47] that finds a spin disordered state in the parameter range $0.25 < J_2/J_1 < 0.34$. In contrast, a study using Schwinger boson mean-field theory [49] observes no spin disordered state and instead finds a direct transition to the spiral AFM for $J_2/J_1 > 0.21$. However, Schwinger bosons may underestimate quantum effects [49, 50]. A quantum field theory suggests that the spin disordered region between the Néel state and spiral AFM is generic to two-dimensional lattices and that the quantum spin liquid shares similarities in its spin gap and spin fluctuations to the Haldane phase found in spin-1 chains [51]. It is interesting that spin-1 formation also occurs in electronic models of quasi-one-dimensional lattices decorated with triangles, whose ground state is in the Haldane phase [25, 52–54]. The nature of triplet formation of triangular structures in other decorated lattices and its relation to real materials remains an open question.

On the decorated honeycomb lattice the highest estimate of the frustration is $J_2/J_1 \approx 0.03$ for $J_{\text{GK}} = -J/3$ and a critical interaction strength $J/W \approx 1$ (Fig. 1). Hence, the ground state of the spin-1 Mott insulator on the decorated honeycomb lattice is Néel ordered.

VIII. CONCLUSION

A spin-1 Mott insulator occurs on the Hubbard model on the decorated honeycomb lattice at two-thirds electron filling, where one would naively expect a correlated metal. The spin-1 Mott insulator can be driven by increasing electronic correlations or moving the lattice closer to the molecular limit (decreasing t_g/t_k). The resulting low-energy effective theory is the spin-1 Heisenberg model on the honeycomb lattice. While the decorated honeycomb lattice is not bipartite, the honeycomb lattice is, and the ground state of the spin-1 Mott insulator is Néel ordered.

An antiferromagnetic intra-triangle spin exchange drives the spin-1 Mott insulator to a spin-0 Mott insulator via a metallic phase. Both insulators are adiabatically connected to the limit of an isolated triangle, where the ground state is a spin-triplet because of an effective Hund's coupling in the basis of trimer orbitals that favors high-spin on a triangle, or a spin-singlet from an effective Coulomb attraction that favors low-spin on a triangle.

In quasi-one-dimensional electronic models spin-triplet formation on a triangle results in the Haldane phase, which is the ground state of the spin-1 Heisenberg chain [25, 52–54]. We propose that spin-1 insulators is general to other lattices decorated with odd-sided polygons.

Doping the Haldane phase in quasi-one-dimensional models leads to spin-triplet superconducting fluctuations

[54]. Two questions arise from this observation. First, are the preformed triplets in the Haldane phase important for driving superconductivity, or does the unconventional superconductivity arise from the Mott insulator? Second, does spin-triplet superconductivity occur in higher dimensions of coupled triangles or is the low dimensionality important? In particular, it is an open question whether superconductivity occurs on the decorated honeycomb lattice in the vicinity of the spin-1 Mott insulator. It has already been shown that f -wave spin-singlet superconductivity can occur near half-filling on the decorated honeycomb lattice [55].

ACKNOWLEDGMENTS

We thank Jason Pillay and Elise Kenny for helpful conversations. This work was supported by the Australian Research Council through Grants No. DP160102425, DP160100060, and DP181006201.

Appendix A: Hubbard U in molecular orbital basis

For any N -ring the single-particle transformation to the molecular orbital basis can be written as

$$\hat{c}_{i\alpha\sigma} \equiv \frac{1}{\sqrt{N}} \sum_m \hat{b}_{im\sigma}^\dagger e^{-i\phi(\alpha-1)m}, \quad (\text{A1})$$

where $\phi = 2\pi/N$, and $m \in [0, N)$ is an index labeling the N molecular orbitals.

The on-site Coulomb repulsion in the molecular orbital basis is given by

$$\hat{H}_i^{U,N} \equiv U \sum_\alpha \hat{n}_{i\alpha\uparrow} \hat{n}_{i\alpha\downarrow} = \frac{U}{N} \sum_{mnp} \hat{b}_{im\uparrow}^\dagger \hat{b}_{in\uparrow} \hat{b}_{ip\downarrow}^\dagger \hat{b}_{i(m+p-n)\downarrow}, \quad (\text{A2})$$

where the identity for Fourier transforms $\frac{1}{N} \sum_\alpha e^{i\phi\alpha(n-m)} = \delta_{mn}$ was used, and hence $(m+n)$ is calculated modulo N . Expanding the terms on the right hand side gives

$$\begin{aligned} \hat{H}_i^{U,N} &= \frac{U}{N} \sum_m \hat{n}_{im\uparrow} \hat{n}_{im\downarrow} \\ &+ \frac{U}{N} \sum_{m \neq n} \left(\hat{n}_{im\uparrow} \hat{n}_{in\downarrow} + \hat{b}_{im\downarrow}^\dagger \hat{b}_{in\uparrow}^\dagger \hat{b}_{im\uparrow} \hat{b}_{in\downarrow} \right) \\ &+ \frac{U}{N} \sum_{m \neq n} \hat{b}_{im\downarrow}^\dagger \hat{b}_{im\uparrow}^\dagger \hat{b}_{in\uparrow} \hat{b}_{i(2m-n)\downarrow} \\ &+ \frac{U}{N} \sum_m \sum_{n \neq n} \sum_{p \neq m,n} \hat{b}_{ip\downarrow}^\dagger \hat{b}_{im\uparrow}^\dagger \hat{b}_{in\uparrow} \hat{b}_{i(m+p-n)\downarrow}. \end{aligned} \quad (\text{A3})$$

The total spin operator can be written as

$$\vec{S}_i^2 = \sum_m \vec{S}_{im} \cdot \vec{S}_{im} + \sum_{m \neq n} \vec{S}_{im} \cdot \vec{S}_{in}, \quad (\text{A4})$$

with the total spin in an orbital given by

$$\vec{S}_{im}^2 \equiv \vec{S}_{im} \cdot \vec{S}_{im} = \frac{3}{4} \sum_{\sigma} \hat{n}_{im\sigma} - \frac{3}{2} \hat{n}_{im\uparrow} \hat{n}_{im\downarrow}, \quad (\text{A5})$$

and the spin exchange interaction between orbitals given by

$$\begin{aligned} \vec{S}_{im} \cdot \vec{S}_{in} &= \frac{1}{4} \sum_{\sigma} \hat{n}_{im\sigma} \hat{n}_{in\sigma} - \frac{1}{2} \hat{n}_{im\uparrow} \hat{n}_{in\downarrow} \\ &\quad - \hat{b}_{im\downarrow}^{\dagger} \hat{b}_{in\uparrow}^{\dagger} \hat{b}_{im\uparrow} \hat{b}_{in\downarrow}, \end{aligned} \quad (\text{A6})$$

where we used that $\vec{S}_{im} = (S_{im}^x, S_{im}^y, S_{im}^z)$ is given by

$$\vec{S}_{im} \equiv \frac{1}{2} \sum_{\sigma\sigma'} \hat{b}_{im\sigma}^{\dagger} \vec{\tau}_{\sigma\sigma'} \hat{b}_{im\sigma'}, \quad (\text{A7})$$

with $\vec{\tau}$ a vector of Pauli matrices. The total number operator is given by

$$\hat{N}_i \equiv \sum_{m\sigma} \hat{n}_{im\sigma}, \quad (\text{A8})$$

and its squared is given by

$$\begin{aligned} \hat{N}_i^2 &= \sum_m \hat{N}_i^2 + \sum_{m \neq n} \hat{N}_i^2 \\ &= \hat{N}_i + 2 \sum_m \hat{n}_{im\uparrow} \hat{n}_{im\downarrow} \\ &\quad + \sum_{m \neq n, \sigma} \hat{n}_{im\sigma} \hat{n}_{in\sigma} + 2 \sum_{m \neq n} \hat{n}_{im\uparrow} \hat{n}_{in\downarrow}. \end{aligned} \quad (\text{A9})$$

Hence, the Hubbard U interaction for an N -ring can be written in the molecular orbital basis as

$$\begin{aligned} \hat{H}_i^{U,N} &= -\frac{U}{N} \vec{S}_i^2 + \frac{U}{4N} \hat{N}_i^2 + \frac{U}{2N} \hat{N}_i - \frac{U}{N} \sum_m \hat{n}_{im\uparrow} \hat{n}_{im\downarrow} \\ &\quad + \frac{U}{N} \sum_{m \neq n} \hat{b}_{im\downarrow}^{\dagger} \hat{b}_{im\uparrow}^{\dagger} \hat{b}_{in\uparrow} \hat{b}_{i(2m-n)\downarrow} \\ &\quad + \frac{U}{N} \sum_m \sum_{n \neq n} \sum_{p \neq m, n} \hat{b}_{ip\downarrow}^{\dagger} \hat{b}_{im\uparrow}^{\dagger} \hat{b}_{in\uparrow} \hat{b}_{i(m+p-n)\downarrow}. \end{aligned} \quad (\text{A10})$$

For $N = 3$, the Hamiltonian for the Hubbard U interaction in the trimer basis is given by Eq. (9) in the main text.

Appendix B: Spin exchange J_{GK} in molecular orbital basis

The intra-triangle spin exchange interaction is given by

$$\hat{H}_i^F \equiv J_{\text{GK}} \left(\sum_{\alpha \neq \beta} \vec{S}_{i\alpha} \cdot \vec{S}_{i\beta} - \frac{1}{4} \hat{n}_{i\alpha} \hat{n}_{i\beta} \right). \quad (\text{B1})$$

The first term can be written as

$$\begin{aligned} \sum_{\alpha \neq \beta} \vec{S}_{i\alpha} \cdot \vec{S}_{i\beta} &= \vec{S}_i^2 - \sum_m \vec{S}_{im}^2 \\ &= \vec{S}_i^2 - \frac{3}{4} \hat{N}_i + \frac{3}{2} \sum_{\alpha} \hat{n}_{i\alpha\uparrow} \hat{n}_{i\alpha\downarrow}, \end{aligned} \quad (\text{B2})$$

and the second term can be written as

$$\frac{1}{4} \sum_{\alpha \neq \beta} \hat{n}_{i\alpha} \hat{n}_{i\beta} = \frac{1}{4} \hat{N}_i^2 - \frac{1}{4} \hat{N}_i - \frac{1}{2} \sum_{\alpha} \hat{n}_{\alpha\uparrow} \hat{n}_{\alpha\downarrow}. \quad (\text{B3})$$

Hence, the spin exchange interaction within a triangle can be written as

$$\hat{H}_i^{\text{GK}} = J_{\text{GK}} \vec{S}_i^2 - \frac{J_{\text{GK}}}{4} \hat{N}_i^2 - \frac{J_{\text{GK}}}{2} \hat{N}_i + 2J_{\text{GK}} \sum_{\alpha} \hat{n}_{i\alpha\uparrow} \hat{n}_{i\alpha\downarrow}. \quad (\text{B4})$$

Transforming the on-site Hubbard term using the results of Appendix A gives Eq. (10) in the main text.

Note that combining the Hubbard U and the spin exchange interaction gives

$$\begin{aligned} \hat{H}_i^U + \hat{H}_i^{\text{GK}} &= -\frac{1}{3}(U - J_{\text{GK}}) \vec{S}_i^2 + \frac{1}{12}(U - J_{\text{GK}}) \hat{N}_i^2 \\ &\quad + \frac{1}{6}(U - J_{\text{GK}}) \hat{N}_i - \frac{1}{3}(U + 2J_{\text{GK}}) \sum_m \hat{n}_{im\uparrow} \hat{n}_{im\downarrow} \\ &\quad + \frac{1}{3}(U + 2J_{\text{GK}}) \sum_m \sum_{n \neq m} \sum_{p \neq m \neq n} \left(\hat{b}_{im\downarrow}^{\dagger} \hat{b}_{im\uparrow}^{\dagger} \hat{b}_{in\uparrow} \hat{b}_{ip\downarrow} + \text{H.c.} \right). \end{aligned} \quad (\text{B5})$$

-
- [1] M. Imada, A. Fujimori, and Y. Tokura, *Rev. Mod. Phys.* **70**, 1039 (1998).
 [2] N. F. Mott, *Rev. Mod. Phys.* **40**, 677 (1968).
 [3] F. C. Zhang and T. M. Rice, *Phys. Rev. B* **37**, 3759 (1988).
 [4] F. C. Zhang and T. M. Rice, *Phys. Rev. B* **41**, 7243 (1990).
 [5] B. J. Powell and R. H. McKenzie, *Rep. Prog. Phys.* **74**, 056501 (2011).
 [6] Y. Tokura and N. Nagaosa, *Science* **288**, 462 (2000).

- [7] Q. Si, R. Yu, and E. Abrahams, *Nat. Rev. Mater.* **1**, 16017 (2016).
 [8] J. Kanamori, *Prog. of Theor. Phys.* **30**, 275 (1963).
 [9] A. Georges, L. d. Medici, and J. Mravlje, *Annu. Rev. Condens. Matter Phys.* **4**, 137 (2013).
 [10] R. Murase, C. F. Leong, and D. M. D'Alessandro, *Inorg. Chem.* **56**, 14373 (2017).
 [11] R. Murase, B. F. Abrahams, D. M. D'Alessandro, C. G. Davies, T. A. Hudson, G. N. L. Jameson, B. Moubarak, K. S. Murray, R. Robson, and A. L. Sutton, *Inorg. Chem.*

- 56**, 9025 (2017).
- [12] C. J. Kingsbury, B. F. Abrahams, D. M. D'Alessandro, T. A. Hudson, R. Murase, R. Robson, and K. F. White, *Cryst. Growth Des.* **17**, 1465 (2017).
- [13] I.-R. Jeon, B. Negru, R. P. Van Duyne, and T. D. Harris, *J. Am. Chem. Soc.* **137**, 15699 (2015).
- [14] L. E. Darago, M. L. Aubrey, C. J. Yu, M. I. Gonzalez, and J. R. Long, *J. Am. Chem. Soc.* **137**, 15703 (2015).
- [15] J. A. DeGayner, I.-R. Jeon, L. Sun, M. Dincă, and T. D. Harris, *J. Am. Chem. Soc.* **139**, 4175 (2017).
- [16] L. M. Henling and R. E. Marsh, *Acta Crystallogr., Sect. C: Struct. Chem.* **70**, 834 (2014), CSD-FAZGIY.
- [17] K. M. Henline, C. Wang, R. D. Pike, J. C. Ahern, B. Sousa, H. H. Patterson, A. T. Kerr, and C. L. Cahill, *Cryst. Growth Des.* **14**, 1449 (2014).
- [18] R. A. Polunin, V. N. Dorofeeva, A. E. Baranchikov, V. K. Ivanov, K. S. Gavrilenko, M. A. Kiskin, I. L. Eremenko, V. M. Novotortsev, and S. V. Kolotilov, *Russ. J. Coord. Chem.* **41**, 353 (2015).
- [19] M. J. Kalmutzki, N. Hanikel, and O. M. Yaghi, *Sci. Adv.* **4**, 10.1126/sciadv.aat9180 (2018).
- [20] H. L. Nourse, R. H. McKenzie, and B. J. Powell, *Phys. Rev. B* **103**, L081114 (2021).
- [21] J. B. Goodenough, *Phys. Rev.* **100**, 564 (1955).
- [22] J. B. Goodenough, *J. Phys. Chem. Solids* **6**, 287 (1958).
- [23] J. Kanamori, *J. Phys. Chem. Solids* **10**, 87 (1959).
- [24] A. C. Jacko, C. Janani, K. Koepernik, and B. J. Powell, *Phys. Rev. B* **91**, 125140 (2015).
- [25] C. Janani, J. Merino, I. P. McCulloch, and B. J. Powell, *Phys. Rev. B* **90**, 35120 (2014).
- [26] G. Kotliar and A. E. Ruckenstein, *Phys. Rev. Lett.* **57**, 1362 (1986).
- [27] F. Lechermann, A. Georges, G. Kotliar, and O. Parcollet, *Phys. Rev. B* **76**, 155102 (2007).
- [28] N. Lanatà, Y. Yao, C.-Z. Wang, K.-M. Ho, and G. Kotliar, *Phys. Rev. X* **5**, 11008 (2015).
- [29] N. Lanatà, Y. Yao, X. Deng, V. Dobrosavljević, and G. Kotliar, *Phys. Rev. Lett.* **118**, 126401 (2017).
- [30] N. Lanatà, T.-H. Lee, Y.-X. Yao, and V. Dobrosavljević, *Phys. Rev. B* **96**, 195126 (2017).
- [31] W. Metzner and D. Vollhardt, *Phys. Rev. Lett.* **62**, 324 (1989).
- [32] J. Bünnemann and F. Gebhard, *Phys. Rev. B* **76**, 193104 (2007).
- [33] N. Lanatà, P. Barone, and M. Fabrizio, *Phys. Rev. B* **78**, 155127 (2008).
- [34] O. Parcollet, M. Ferrero, T. Ayral, H. Hafermann, I. Krivenko, L. Messio, and P. Seth, *Comput. Phys. Commun.* **196**, 398 (2015), version 1.4.
- [35] P. Seth, I. Krivenko, M. Ferrero, and O. Parcollet, *Comput. Phys. Commun.* **200**, 274 (2016).
- [36] P. E. Blöchl, O. Jepsen, and O. K. Andersen, *Phys. Rev. B* **49**, 16223 (1994).
- [37] ARPACK-NG, <https://github.com/opencollab/arpack-ng>, [Online; accessed July 2017].
- [38] I. Krivenko, ezARPACK - a C++ ARPACK-NG wrapper compatible with multiple matrix/vector algebra libraries: Release 0.9 (2020).
- [39] W. F. Brinkman and T. M. Rice, *Phys. Rev. B* **2**, 4302 (1970).
- [40] J. C. Slater, *Phys. Rev.* **82**, 538 (1951).
- [41] M. Fabrizio, *Phys. Rev. B* **95**, 075156 (2017).
- [42] M. M. Wysokiński and M. Fabrizio, *Phys. Rev. B* **95**, 161106 (2017).
- [43] J. Merino, A. C. Jacko, A. L. Khosla, and B. J. Powell, *Phys. Rev. B* **94**, 205109 (2016).
- [44] B. J. Powell, J. Merino, A. L. Khosla, and A. C. Jacko, *Phys. Rev. B* **95**, 94432 (2017).
- [45] J. Merino, A. C. Jacko, A. L. Khosla, and B. J. Powell, *Phys. Rev. B* **96**, 205118 (2017).
- [46] S.-S. Gong, W. Zhu, and D. N. Sheng, *Phys. Rev. B* **92**, 195110 (2015).
- [47] P. H. Y. Li and R. F. Bishop, *Phys. Rev. B* **93**, 214438 (2016).
- [48] J. Merino, A. C. Jacko, A. L. Khosla, A. Ralko, and B. J. Powell, *AIP Adv.* **8**, 101430 (2018).
- [49] J. Merino and A. Ralko, *Phys. Rev. B* **97**, 205112 (2018).
- [50] D.-V. Bauer and J. O. Fjærestad, *Phys. Rev. B* **96**, 165141 (2017).
- [51] Y. A. Kharkov, J. Oitmaa, and O. P. Sushkov, *Phys. Rev. B* **98**, 144420 (2018).
- [52] C. Janani, J. Merino, I. P. McCulloch, and B. J. Powell, *Phys. Rev. Lett.* **113**, 267204 (2014).
- [53] H. L. Nourse, I. P. McCulloch, C. Janani, and B. J. Powell, *Phys. Rev. B* **94**, 214418 (2016).
- [54] S. Reja and S. Nishimoto, *Sci. Rep* **9**, 2691 (2019).
- [55] J. Merino, M. F. López, and B. J. Powell, *Phys. Rev. B* **103**, 094517 (2021).